horticulturae

MDPI

Article

Brassinosteroid Is Associated with Floral Bud Dormancy and Flowering via the Transcription Factor BZR1-3 in *Camellia yuhsienensis*

Hui Qian [1,2], Jin Feng [1,2], Yu Dong [1,2], Yihong Chang [1,2], Wenfang Gong [1,2] and Deyi Yuan [1,2,*]

[1] State Key Laboratory of Woody Oil Resources Utilization, Key Laboratory of Cultivation and Protection for Non-Wood Forest Trees of the Ministry of Education, Central South University of Forestry and Technology, Changsha 410004, China; qianhuiboshi@126.com (H.Q.); xijin1006@163.com (J.F.); dongyu888@163.com (Y.D.); chang-yihong@csuft.edu.cn (Y.C.); gwf018@126.com (W.G.)
[2] Yuelushan Laboratory Non-Wood Forests Variety Innovation Center, Changsha 410004, China
* Correspondence: yuan-deyi@163.com

Highlights

What are the main findings?

- Spring-flowering *Camellia yuhsienensis* maintains high BR levels in floral buds, which is associated with prolonged dormancy and delayed flowering until spring, whereas autumn–winter flowering ecotypes show declining BR and flower without dormancy.
- BZR1-3 is identified as a BR-responsive transcription factor which correlates with bud dormancy and flowering.

What are the implications of the main findings?

- Exogenous EBR regulates flowering in a concentration-dependent manner, offering a potential strategy for manipulating flowering time in oil camellias.
- BR-BZR1-3 pathway provides a molecular target for breeding spring-flowering cultivars.

Abstract

Oil camellia (*Camellia oleifera*), one of the world's four major oil woody species, faces a productivity bottleneck due to its autumn–winter flowering habit, which renders floral buds susceptible to cold damage and reduces yield. Although a spring flowering ecotype of *Camellia yuhsienensis* (CYUH) avoids this disadvantage, the underlying mechanism remains elusive. Brassinosteroid (BR) is a key phytohormone, yet its role in flowering-time regulation of oil camellias remain largely uncharacterized. To elucidate the spring flowering mechanism, we compared two wild ecotypes with synchronous floral bud differentiation but opposite flowering phenologies: the autumn–winter flowering plants CYUH (AF1) and the spring flowering plants CYUH (SF3). SF3 accumulated higher BR levels during autumn and winter, maintaining floral bud dormancy and delaying flowering until spring. In contrast, AF1 exhibited a progressive decline in BR and flowered directly without dormancy. Treatment with 0.5 mg/L exogenous EBR reduced BR levels and accelerated flowering, whereas 2 mg/L exogenous EBR increased BR levels and delayed flowering in both AF1 and SF3, indicating a concentration-dependent association of BR with flowering. Transcriptome sequencing and quantitative RT-PCR identified BZR1-3 as a candidate transcription factor of BR signaling, whose high BR-induced upregulation correlated with delayed flowering. Collectively, these findings suggest that BZR1-3 is potentially involved in BR to coordinate floral bud dormancy and flowering, offering a foundation for breeding spring flowering cultivars in oil camellias.

Check for updates

Academic Editors: Jae Hwan Lee, Yoon-Jung Hwang and Ki-Byung Lim

Received: 16 September 2026
Revised: 14 November 2026
Accepted: 16 November 2026
Published: 18 November 2026

Copyright: © 2026 by the authors. Licensee MDPI, Basel, Switzerland. This article is an open access article distributed under the terms and conditions of the Creative Commons Attribution (CC BY) license.

Keywords: *Camellia yuhsienensis*; BR; BZR1-3; DRM1; dormancy; flowering

1. Introduction

Precise regulation of flowering time is essential for maximizing reproductive success and sustaining vegetative growth [1]. Flowering is orchestrated through the dynamic integration of external environmental signals, such as photoperiod, temperature, and vernalization [2], and internal plant factors, including hormonal status, carbohydrate availability [3], and developmental age [4]. In perennial woody plants, dormancy serves as a critical adaptive strategy that delays flowering and protects floral buds from winter damage by repressing precocious bud break before spring onset [5]. Floral bud dormancy is broadly categorized into three types: paradormancy, imposed by signals from adjacent organs; endodormancy, driven by internal physiological cues that prevent growth during seasonal transitions [6]; and ecodormancy, triggered by external factors such as cold or drought stress [7]. In trees, the cessation of floral bud growth and subsequent bud set are governed by synergistic interactions between environmental cues and endogenous autonomous pathways [8]. These interactions are indispensable for entering dormancy and ultimately establish the dormant state [9]. Among endogenous regulators, phytohormones occupy a central position. In particular, they have been mechanistically linked to the control of flowering time [10], as well as to dormancy control [11]. For example, ethylene generally promotes floral bud dormancy [7]. In contrast, gibberellins (GA) promote dormancy release and trigger floral bud break [12]. In pears (*Pyrus pyrifolia*), early defoliation induces auxin redistribution, promoting floral bud paradormancy release [13]. Taken together, these findings highlight the central role of phytohormones in coordinating dormancy and flowering transitions in woody plants.

Building on the well-established connection between phytohormonal pathways and flowering regulation, brassinosteroid (BR) emerges as a versatile plant phytohormone orchestrating diverse aspects of reproductive timing [14]. In Arabidopsis (*Arabidopsis thaliana*), attenuation of BR upregulates *FLOWERING LOCUS C* (*FLC*) expression and delays flowering [15]. Conversely, BR accelerates flowering by suppressing a negative regulator of floral transition [16]. In tobacco (*Nicotiana tabacum*), cold promotes flowering by activating BR, and overexpression of the BR receptor NtBRI1 induces early flowering [17]. The BR-responsive transcription factor ZmBES1/BZR1-9 promotes early flowering when expressed in both *Arabidopsis* and rice (*Oryza sativa*) [18]. In contrast, in tea plants (*Camellia sinensis*), a non-flowering mutant line exhibits elevated BR levels and increased *CsBZR2* expression, which directly suppresses flowering [19]. Collectively, these species-specific observations underscore that BR exerts divergent effects on flowering time across species.

Given the species-specific effects of BR on flowering timing observed in various plants, it is of great interest to investigate this process in oil camellia (*Camellia oleifera*), a species that is one of the world's four major woody oil tree species [20]. It is predominantly cultivated in subtropical regions of China and is honored as "Eastern Olive Oil" [21]. Precise flowering timing is crucial for oil camellias to avoid unfavorable conditions and ensure reproductive success [22]. However, cultivated oil camellias typically exhibit autumn–winter flowering phenology [23]. During this period, floral buds are frequently subjected to cold stress [24], including fluctuating low temperatures, frost damage, and excessive precipitation [25]. Such abiotic stresses severely compromise key reproductive processes, including pollen germination, stigma receptivity, pollination efficiency, and subsequent fertilization [26]. Adding to this challenge, the majority of oil camellia cultivars exhibit genetic self-incompatibility [27]. Cold stress in autumn and winter further diminishes cross-

pollination effectiveness [10]. Consequently, these interacting biotic and abiotic constraints frequently result in prolific flowering but markedly low fruit set [28], ultimately imposing a critical bottleneck on yield stability and productivity. Therefore, deciphering how floral buds perceive and respond to environmental cues is essential for alleviating the yield bottleneck in oil camellias.

Notably, a spring flowering ecotype of oil camellia (*Camellia yuhsienensis*, CYUH) has been identified, which effectively circumvents these climatic constraints [29], representing a promising genetic resource for flowering time improvement. To elucidate this mechanism, we selected two wild ecotypes of CYUH with similar genetic backgrounds, namely the autumn–winter flowering plants CYUH (AF1), full blooming in December and the spring flowering plants CYUH (SF3), full blooming in March. To systematically track their physiological divergence, we collected floral buds across six stages from June to March of the following year. Using these two contrasting ecotypes, we first conducted comparative analyses of flowering phenology and phytohormone dynamics across six stages. These analyses revealed the correlation between the dormancy-to-flowering transition and dynamic changes in BR levels. Building upon these findings, we performed transcriptome sequencing and quantitative real-time PCR (qRT-PCR) to identify candidate genes involved in BR-mediated dormancy and flowering regulation. We then applied exogenous EBR treatments applied to AF1 and SF3 to functionally assess the role of BR in mediating the dormancy-to-flowering transition. By integrating these multi-layered assays, this study provides insights into how BR is potentially involved in regulating floral bud dormancy and flowering in oil camellias.

2. Materials and Methods

2.1. Plant Materials

The autumn–winter flowering plants CYUH (AF1) and spring flowering plants CYUH (SF3) ecotypes of *C. yuhsienensis* (CYUH) were collected from Dongfeng Forest Farm, Liping County, Guizhou Province, China (109°12′ E, 26°20′ N). AF1 and SF3, representing distinct flowering ecotypes were selected for comparative analysis. AF1 reached full bloom in late December, while SF3 reached full bloom in March of the following year. Floral buds were systematically sampled at 9:00 AM across six developmental stages (P1–P6), with eight biological replicates per stage. To ensure independent biological replicates, all floral buds were collected from independent trees of AF1 and SF3 in field condition. Specifically, floral buds from both AF1 (P1–P5) and SF3 (P1–P6) were collected at each equivalent stage. P1, late June; P2, early September; P3, mid-October; P4, late November; P5, late December; P6, early March of the following year. At the divergent stages (P4 and P5), samples from AF1 consisted of a mixture of opened flowers and unopened floral buds (based on their actual flowering rate), whereas samples from SF3 consisted exclusively of unopened dormant buds. For SF3, the transition from dormancy (P5) to full bloom (P6) was further subdivided into eight consecutive transitional periods (P5-1 to P5-8) to capture dynamic morphological and molecular changes. All collected tissues were immediately flash-frozen in liquid nitrogen and stored at −80 °C until further analysis.

2.2. Observation of Flowering Rate

Flowering progression in AF1 and SF3 was monitored continuously from June 2022 to March 2023 in field condition. Observations covered the six stages (P1–P6) as defined above. For SF3, the eight transitional sub-stages (P5-1 to P5-8) bridging P5 and P6 were additionally monitored. At each stage and sub-stage, eight independent branches (biological replicates) bearing at least 25 floral buds were selected from the sampled trees of AF1 and SF3. The number of fully opened flowers was recorded for each branch. The flowering rate was

calculated for each biological replicate as the percentage of opened flowers relative to the total number of floral buds on that branch. To account for repeated observations over time, data were analyzed using a two-way repeated-measures ANOVA (with branch identity as the subject), followed by Tukey's HSD test. The number of buds were removed for molecular sampling, but a minimum of 25 unopened buds per branch were strictly maintained for phenotyping. The eight independent branches served as the biological replicates (n = 8) to generate the distribution and average flowering rates presented in the figures.

2.3. Floral Bud Paraffin Sectioning

Floral buds collected from independent trees of AF1 and SF3 in field condition, representing five stages (P1–P5), were subjected to histological sectioning. Freshly harvested buds were immediately fixed in Carnoy's fixative (3:1 *v/v* anhydrous ethanol: glacial acetic acid) for histological preservation. For permanent section preparation, fixed samples were subjected to graded ethanol dehydration (30%, 50%, 70%, 85%, 95%, 100%), followed by xylene clearing with transitional solutions (1:1 ethanol: xylene to pure xylene). Paraffin infiltration was accomplished through incremental temperature incubation, starting with 1:1 xylene: paraffin at 40 °C and increasing by 5 °C every 30 min to 60 °C, followed by four changes in pure paraffin at 2 h intervals. Embedded blocks were then solidified, trimmed, and sectioned using standard microtomy protocols. Sections were stained with safranin and fast green for 10 min each for histological visualization. Stained sections were observed and imaged under a Leica DMi8 light microscope.

2.4. Phytohormone Quantification

Phytohormone levels—including abscisic acid (ABA), indole-3-acetic acid (IAA), cytokinin (CTK), gibberellin A_3 (GA_3), and brassinosteroid (BR)—were quantified in AF1 and SF3 floral buds. Samples were homogenized in liquid nitrogen, extracted with 80% methanol containing 1 mmol/L 2-tert-butyl-4-methylphenol (BHT), and purified using C18 solid-phase extraction cartridges. Following solvent evaporation under nitrogen, residues were reconstituted in a diluent containing 0.1% Tween-20, 0.1% gelatin, and phosphate-buffered saline (PBS, pH 7.5).

Phytohormone concentrations were quantified using commercial enzyme-linked immunosorbent assay (ELISA) kits (Ruixin Biotech, Quanzhou, China). The kit catalogue numbers were RXJ1401617PL for BR, RXJ1401520PL for ABA, RXJ1401005PL for IAA, JRX911356 for CTK, and RXJ1401607PL for GA_3. According to the manufacturer's validation, the recovery rate ranges from 85% to 115%. The calibration ranges were set between 0.1 and 20 ng/mg for BR, 0.15 and 50 ng/mg for ABA, 12.5 and 200 ng/mg for IAA, and 0.2 and 100 ng/mg for both GA_3 and CTK. Optical density (OD) was measured at 450 nm using a microplate reader (RT-6100 was manufactured by Rayto Life and Analytical Sciences Co., Ltd., Shenzhen, China). Standard curves were generated according to the manufacturer's instructions, and phytohormone contents were calculated as ng/mg fresh weight (FW). Specifically, post-treatment BR measurements are referred to as assay-defined BR immunoreactivity.

2.5. Transcriptome Sequencing and Comparative Analysis

Comparative transcriptomic profiling was conducted of floral buds from AF1 of five stages (P1–P5) and SF3 of six stages (P1–P6) in field condition. The floral bud samples were sequenced using the Illumina platform (Biomarker Technologies, Beijing, China). Each sample comprised four biological replicates. Total RNA was extracted and assessed for quality, followed by library construction and RNA sequencing on the Illumina platform. After sequencing quality control, a total of 328.45 Gb of clean data was obtained, with the Q30 base percentage for each sample being no less than 96.28%. Clean reads were aligned

to the assembled chromosome-level reference genome of diploid *Camellia yuhsienensis* using HISAT2 (version 2.2.1), with mapping rates ranging from 83.06% to 87.57%. The genomic data have been deposited in the National Genomics Data Center (NGDC/GSA) under BioProject ID PRJCA079697. Gene expression levels were quantified using feature Counts and normalized as FPKM (Fragments Per Kilobase of transcript per Million mapped reads) for visualization. However, differentially expressed genes (DEGs) were identified using DE-Seq2 based on raw, unnormalized read counts, with the thresholds of $|\log2FoldChange| \geq 1$ and FDR < 0.01. The comparisons were performed between AF1 and SF3 at each stage (P1 to P5), as well as across the dormancy-to-flowering transition in SF3 (P5 vs. P6). The resulting DEGs were subjected to Kyoto Encyclopedia of Genes and Genomes (KEGG) pathway enrichment analyses.

2.6. Quantitative Rt-Pcr Validation

Quantitative RT-PCR (qRT-PCR) analyses were performed to validate expression patterns of candidate genes under BR treatment and across developmental transitions. For developmental profiling, floral buds of the spring flowering plants CYUH (SF3) were collected during the critical P5-to-P6 dormancy-release phase, with four biological replicates per sub-stage (P5-1 to P5-8) from independent trees of SF3 in field condition (n = 4). For BR-response assays, floral buds of AF1 and SF3 were harvested at 2, 9, 16, 23, and 30 days after treatments (DAT), with four biological replicates per timepoint (n = 4). Total RNA was extracted using TRIzol reagent from Thermo Fisher Scientific (Waltham, MA, USA), reverse transcribed with Prime Script RT kit from Takara Bio Inc. (Shiga, Japan), and amplified on a QuantStudio 6 Flex system using SYBR Green chemistry from Applied Biosystems (Foster City, CA, USA). *Elongation factor 1α* (*EF1α*) was used as the reference gene. Reaction specificity was confirmed by melt curve analysis, and relative expression levels were calculated using the 2-ΔΔCt method.

2.7. Exogenous EBR Treatments and Flowering Phenotyping

To assess the regulatory role of brassinosteroid (BR) in flowering induction, foliar spray treatments were applied to detached branches of the autumn–winter flowering plants CYUH (AF1) and the spring flowering plants CYUH (SF3). The experiments were initiated approximately 45 days before full bloom for both AF1 and SF3 in field conditions (mid-October for AF1 and mid-January for SF3). At the time of treatment, the floral buds of both ecotypes were in the unopened bud stage, and no artificial prior chilling was applied. The detached branches were hydroponically cultured in distilled water under controlled long-day conditions (16 h light/8 h dark) at 16 °C, with the water replaced daily and the root tips trimmed by 1 mm to maintain growth. Two exogenous 24-epibrassinolide (EBR) concentrations were tested: low-concentration (0.5 mg/L) and high-concentration (2 mg/L). To facilitate the dissolution of the highly hydrophobic EBR in water, it was first dissolved in a minimal volume of ethanol before being diluted with distilled water. The final ethanol concentration in the spray solution did not exceed 0.1% (*v*/*v*). Control (CK) detached branches were sprayed with distilled water without EBR. The pH of all treatment solutions was adjusted to 6.5. Foliar spraying was performed at 9:00 AM on day 1 and day 4 after hydroponics, applied until the leaf surfaces were uniformly moistened. Flowering rates were recorded at five time points (2, 9, 16, 23, and 30 days) after the EBR application days after treatments (DAT), with eight biological replicates per treatment group.

2.8. Protein Structural Modeling

Three-dimensional structural modeling of BZR family proteins (BZR1-1, BZR1-2, BZR1-3, BZR1-4, BZR2, CsBZR1, AtBZR1, and NtBZR1) was performed using SWISS-MODEL

(https://swissmodel.expasy.org/), which applies homology-based modeling against its curated template library.

2.9. Conserved Motif Analysis

To identify the conserved motifs among the BZR family proteins, the amino acid sequences of BZR family proteins (BZR1-1, BZR1-2, BZR1-3, BZR1-4, BZR2, CsBZR1, AtBZR1, and NtBZR1) were subjected to motif analysis using the MEME Suite (version 5.5.9) online server (https://meme-suite.org/meme/tools/meme, accessed on 15 May 2026).

3. Results

3.1. Morphological Synchrony but Contrasting Flowering Phenologies Between Af1 and Sf3

To elucidate the mechanisms regulating flowering time in oil camellias, we performed comparative analyses of two contrasting ecotypes of *Camellia yuhsienensis* (CYUH), the autumn–winter flowering plants CYUH (AF1) and spring flowering plants CYUH (SF3), across six key developmental stages under field conditions: late June (P1), early September (P2), mid-October (P3), late November (P4, autumn), late December (P5, winter), and early March of the following year (P6, spring) (Figure 1A). Paraffin sectioning revealed that both AF1 and SF3 initiated floral organ differentiation at P1 (Figure 1B), and synchronously completed embryonic development by P4 and P5, reaching the mature embryo sac stage (Figure 1C–F).

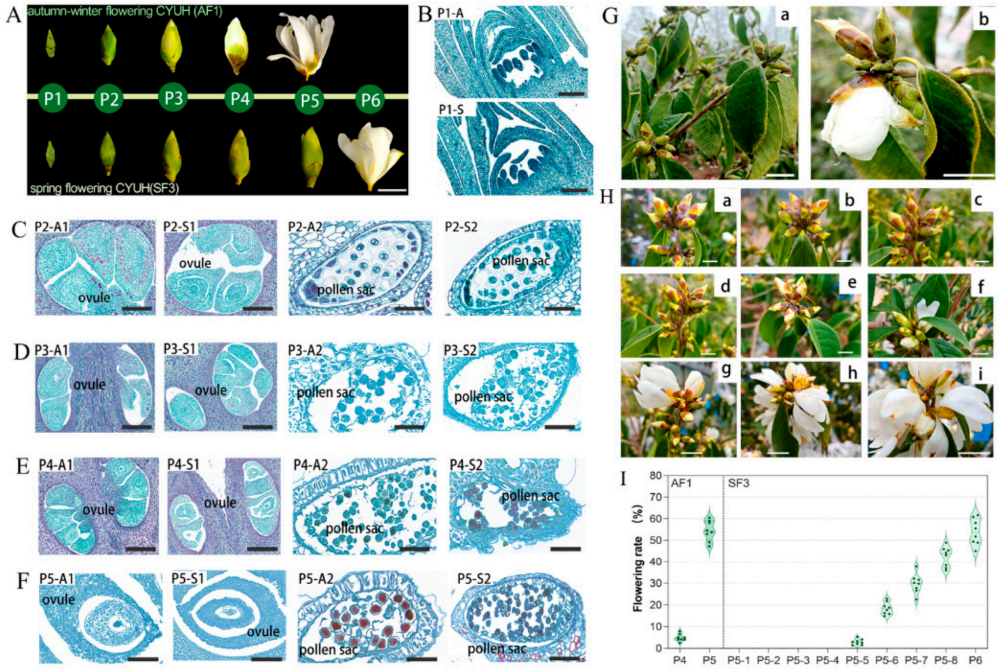


Figure 1. Morphological and cytological analyses of AF1 and SF3 floral buds. (**A**) Morphological changes in floral buds across six developmental periods (P1–P6) in AF1 (autumn–winter flowering plants CYUH) and SF3 (spring flowering plants CYUH). P1, late June; P2, early September; P3, mid-October; P4, late November; P5, late December; P6, early March of the following year. Scale bar, 1 cm. (**B**) Paraffin sections of floral buds at P1. Scale bar, 5 μm. A, AF1; S, SF3. Scale bar, 5 μm. (**C**–**F**) Paraffin sections of floral buds from P2 to P5. A1/S1: ovule development of AF1 and SF3; A2/S2: pollen-sac development of AF1 and SF3. Scale bar, 5 μm. (**G**) Diagrams of CYUH buds in winter (P5). (**a**), spring flowering buds in dormancy (SF3); (**b**) bloomed autumn–winter flowering buds (AF1). Scale bar, 2 cm. (**H**) Nine periods of spring flowering CYUH (SF3). (**a**–**h**) P5-1 to P5-8; (**i**) P6. Scale bar, 1 cm. (**I**) Flowering rates between AF1 and SF3 from P4 to P6. P5-1 to P5-8 represent randomly selected dates between P5 and P6 in SF3. Data are mean ± SD (n = 8).

To capture the dynamic changes during the P5-to-P6 transition in SF3, we subdivided this period into eight sub-stages, designated P5-1 to P5-8. Despite this morphological synchrony in reproductive development (Figure 1B–F), their flowering phenologies differed markedly. AF1 initiated flowering at P4, whereas SF3 initiated flowering at P5-5. AF1 reached full bloom (>50% flowering rate) in late December (P5), while SF3 reached full bloom (>50% flowering rate) in early March of the subsequent year (P6). After completing floral bud differentiation, SF3 floral buds remained in a prolonged dormant [30] and unopened state after P5 and progressively reached full bloom with the onset of spring (P6). In contrast, AF1 bypassed this prolonged dormant phase and reached full bloom at P5. (Figure 1G–I).

3.2. Comparative Phytohormone Dynamics Between Af1 and Sf3

To determine whether phytohormone dynamics contribute to the divergent flowering phenologies between AF1 and SF3, we quantified the contents of major phytohormones in floral buds across key developmental stages. During the early synchronized stages (P1–P3), the fluctuation rhythms of ABA, CTK, GA3, and IAA lacked significant parallelism between AF1 and SF3. Furthermore, these hormones exhibited non-regulatory fluctuations lacking clear directional trends during the critical divergence stages (P4 and P5) and the subsequent flowering transition in SF3 (P5–P6) (Figure 2A–D). Specifically, ABA increased in both flowering AF1 and dormant SF3, with no difference between SF3's dormant (P5) and blooming (P6) stages. CTK fluctuated minimally between the dormant stage (P4) and the blooming stage in SF3. Similarly, GA3 and IAA showed no significant fluctuations in AF1 (P4–P5) and lacked a clear directional trend aligning with dormancy-to-flowering transition (P4–P6) in SF3.

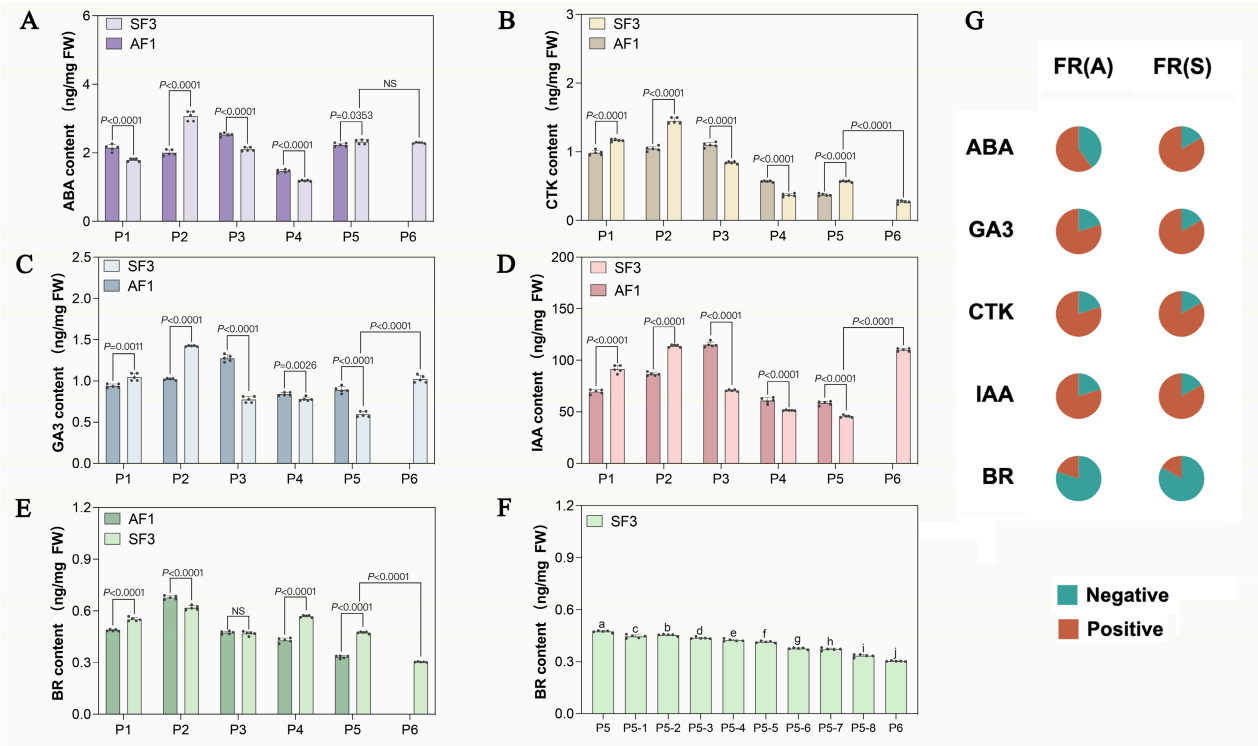


Figure 2. ABA, CTK, GA3, IAA, BR content and correlation analysis. (**A**–**E**) ABA, CTK, GA3, IAA, BR content across six developmental periods (P1–P6). Autumn–winter flowering mutant CYUH, AF1; spring flowering CYUH, SF3. Data are mean ± SD (n = 5). (**F**) BR content in SF3 from P5 to P6. Different letters indicate significant differences (a, highest; i, lowest; one-way ANOVA with Tukey's

HSD test; n = 5). (**G**) Correlation analysis between the BR, IAA, CTK, GA3 and ABA contents and flowering rates. (S) and (A) stand for SF3 and AF1, respectively. FR(S), the flowering rate of SF3. FR(A), the flowering rate of AF1. Green indicates negative correlations, red indicates positive correlations.

In contrast, BR levels exhibited a distinct pattern: following parallel trajectories from P1 to P3, they diverged sharply at P4 and P5, coinciding with the onset of phenological divergence. Specifically, BR concentrations decreased continuously during the flowering periods in AF1 (P4–P5) and SF3 (P5–P6), whereas they remained at a significantly higher level in dormant SF3 buds compared to flowering AF1 buds during the divergence stages (P4–P5) (Figure 2E). During the transition from floral bud dormancy (P5) to full bloom (P6) in SF3, BR levels progressively declined across eight intermediate time points (P5-1 to P5-8) (Figure 2F), showing an inverse correlation with advancing flowering (Figure 1G). Notably, comparably low BR concentrations were observed at full bloom in both ecotypes, corresponding to P5 in AF1 and P6 in SF3, respectively (Figure 1E,F). Overall, BR exhibited a monophasic decline as flowering progressed, and its levels were significantly negatively correlated with flowering rate in both AF1 and SF3 (Figure 2G). These results suggest that BR acts as a potential negative regulator of flowering, associated with sustaining floral bud dormancy and preventing precocious flowering.

3.3. Transcriptomic Profiling of BR Signaling Genes

To investigate the dynamic transcriptional changes underlying the contrasting flowering phenologies between AF1 and SF3, we performed RNA-seq analysis on floral buds collected at six developmental stages (P1–P6). Principal component analysis (PCA) of the transcriptome data revealed that the first two principal components (PC1 and PC2) accounted for 21.09% and 14.37% of the total variance, respectively. Biological replicates within each stage clustered tightly together, indicating high data quality and reproducibility (Figure S1). A Venn diagram was used to analyze the shared and stage-specific DEGs across the five comparison groups (P1–P5), and a total of 724 common DEGs were identified in all five developmental periods. Regarding stage-specific DEGs, 1443, 2167, 1128, 1345, and 1100 were uniquely detected at P1, P2, P3, P4, and P5, respectively (Figure 3A). The bar chart further quantified the total, upregulated, and downregulated DEGs in each comparison. Overall DEG counts increased progressively from P1 to P5, peaking at P5 (6804 total; 3326 upregulated and 3478 downregulated), coinciding with the pronounced divergence in flowering time between AF1 and SF3. Notably, the dormancy-to-flowering transition in SF3 (P5 vs. P6) exhibited the most pronounced transcriptional divergence, yielding 12,716 DEGs (6515 upregulated and 6201 downregulated) (Figure 3B).

KEGG pathway analysis of the Environmental Information Processing category uncovered multiple pathways linked to environmental signal perception and transduction, among which plant phytohormone signal transduction emerged as the most significantly enriched pathway across all developmental periods (Figures S2–S7). Within this pathway, both upregulated and downregulated DEGs increased progressively from P1 to P5, with maximal enrichment observed at P4 (52 upregulated, 91 downregulated) and P5 (50 upregulated, 85 downregulated). During the dormancy-to-flowering transition in SF3 (P5 vs. P6), plant hormone signal transduction DEGs showed marked enrichment, with 161 upregulated and 184 downregulated (Figure 3C,D). At the divergent stages (P4 and P5), AF1 samples contained both opened flowers and unopened buds, whereas SF3 samples consisted exclusively of unopened buds; thus, the observed hormone and transcript differences may partially reflect this variation in tissue composition.

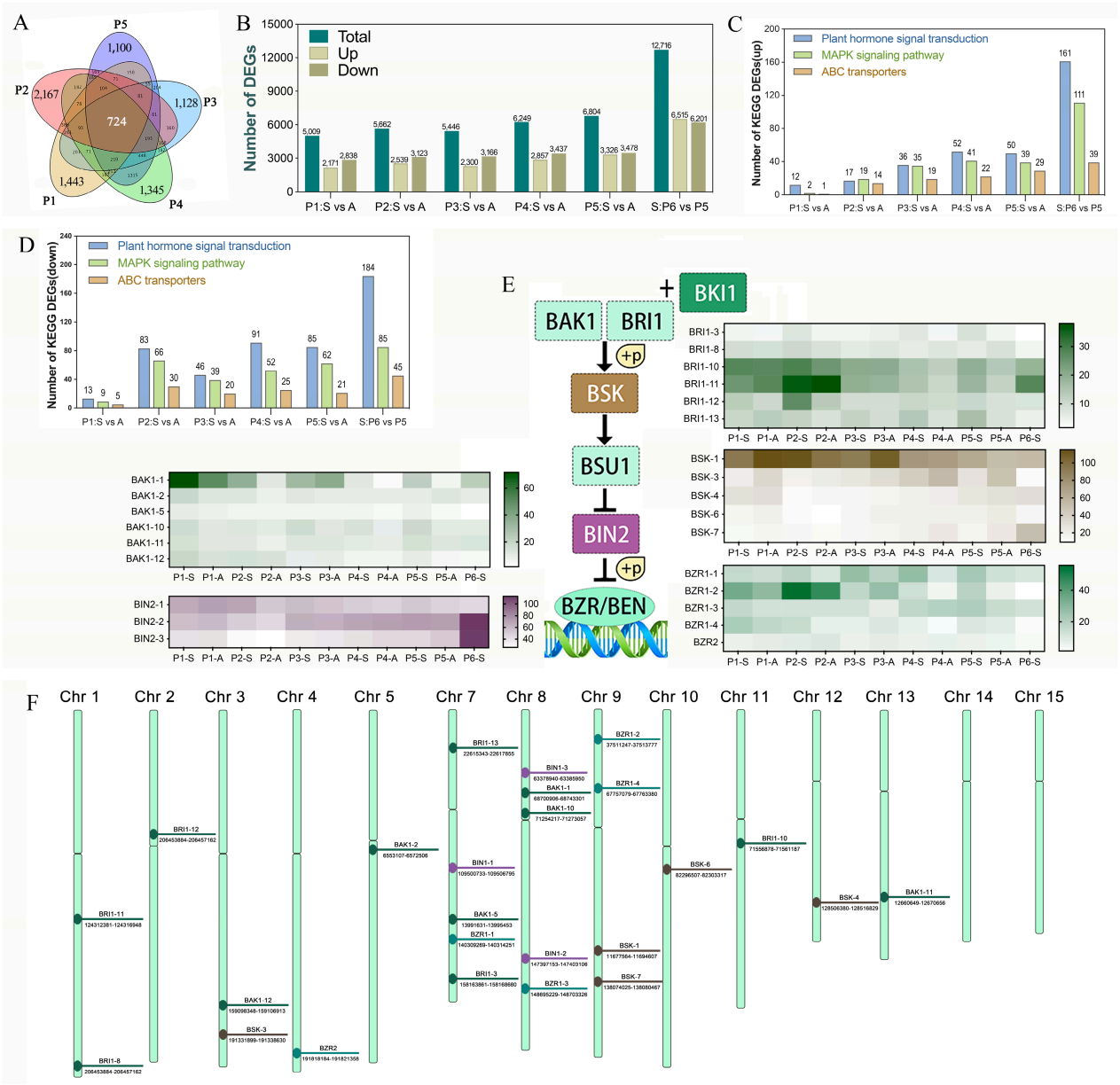


Figure 3. Transcriptomic profiling of BR signaling genes. (**A**) Venn diagram of differentially expressed genes (DEGs) between AF1 and SF3 floral buds across five developmental periods (P1–P5). (**B**) Numbers of DEGs between AF1 and SF3 floral buds. A: AF1; S: SF3. (**C**) Numbers of upregulated DEGs assigned to the "Environmental Information Processing" KEGG category in AF1 and SF3 floral buds. (**D**) Numbers of downregulated DEGs assigned to the "Environmental Information Processing" KEGG category in AF1 and SF3 floral buds. (**E**) Transcriptional profiles of key BR signaling genes in AF1 and SF3 floral buds across P1–P6. (**F**) Chromosome localization of BR signal genes. The *BSK* genes are marked in color coffee, the *BIN* genes in purple, the *BRI* and *BAK* genes in green and the *BZR* genes in cyan.

Notably, a total of 25 BR signal transduction genes were identified as differentially expressed genes (DEGs), encompassing core components distributed across the entire signaling cascade. The BR signaling pathway initiates at the plasma membrane, where the receptor kinase BRI1 and its co-receptor BAK1 perceive BR ligands, whereas the inhibitory protein BKI1 maintains the receptor complex in an inactive state [31]. Upon BR perception, BKI1 is phosphorylated and dissociates from BRI1, thereby activating the receptor complex [32]. Six DEGs were assigned to BRI1 and an equal number to BAK1, indicating a robust transcriptional response at the perception level. The activated BRI1 subsequently

phosphorylates the downstream kinases BSK and BSU1, which in turn inhibit the GSK3-like kinase BIN2 [33]. Specifically, five DEGs were mapped to *BSK*, while three DEGs corresponded to *BIN2*. Notably, five DEGs were identified for BZR1, a pivotal transcription factor downstream of BR signaling [14] (Figure 3E). Furthermore, the 25 DEGs were distributed across 13 of the 15 chromosomes (Figure 3F).

3.4. BZR1-3 Is Associated with Floral Bud Dormancy and Flowering in Response to BR

Among the five *BZR1* homologs identified, *BZR1-3* displayed the most pronounced expression differences between AF1 and SF3 floral buds, accumulating steadily during floral bud dormancy (P4–P5) but being sharply downregulated upon full bloom (P6) in SF3 floral buds. In SF3, *BZR1-3* expression decreased significantly from dormant P5 to full bloom P6 ($p < 0.0001$). Notably, both ecotypes converged to comparable *BZR1-3* expression levels at their respective peak flowering stages (Figure 4A–E). In SF3, the time-course spanning P5–P6 transition further revealed that *BZR1-3* expression was progressively downregulated, closely mirroring the concurrent decline in BR levels and supporting its inverse correlation with flowering progression (Figures 1I, 2F and 4F). Sequence alignment demonstrated high conservation among BZR proteins across species, including *CsBZR1* from *Camellia sinensis*, *AtBZR1* from *Arabidopsis thaliana*, and *NtBZR1* from *Nicotiana tabacum* (Figure S8). Protein structure modeling further predicted a conserved helix-turn-helix (HTH) DNA-binding domain, represented by continuous α-helical regions (colored blue and cyan), which is characteristic of the BZR protein family (Figure 4G).

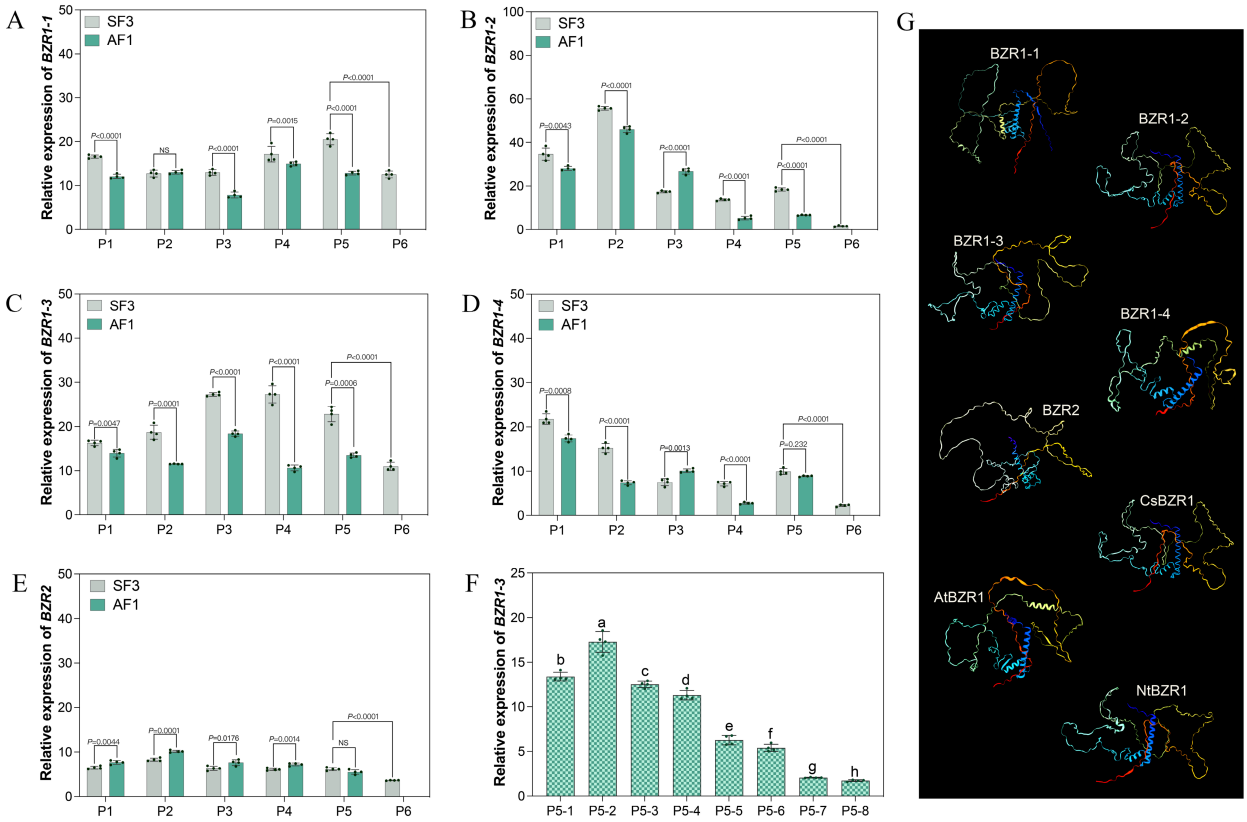


Figure 4. Expression analysis and structural modeling of *BZR1-3*. (**A**–**E**) Transcriptomic expression of *BZR1* homologs in AF1 and SF3 floral buds across P1-P6. Data are mean ± SD (n = 4). (**F**) qRT-PCR analysis of *BZR1-3* expression in SF3 floral buds from P5-1 to P5-8. *EF1α* was used as the internal reference. Different letters indicate significant differences (a, highest; h, lowest; one-way ANOVA with Tukey's HSD test; n = 4). (**G**) Predicted protein structures of BZR1 homologs, colored by secondary structure.

3.5. Exogenous EBR Treatments Regulate Flowering in a Concentration-Dependent Manner

To functionally test BR is associated with floral bud dormancy and flowering timing, we applied exogenous EBR treatments at two concentrations: low-concentration (EBR-L, 0.5 mg/L) and high-concentration (EBR-H, 2 mg/L) to both AF1 at mid-October and SF3 at mid-January. Flowering phenotypes were monitored at 2, 9, 16, 23, and 30 days after exogenous EBR treatments (DAT) (Figure 5A,B). Compared with the control group (CK), the exogenous high-concentration EBR treatments group (EBR-H) significantly delayed flowering, with no visible floral buds observed until 23 DAT. In contrast, the exogenous low-concentration EBR treatments group (EBR-L) accelerated flowering initiation, achieving a flowering rate exceeding 10% at 16 DAT, while the CK group remained below 10% at the same time point ($p < 0.0001$). At 30 DAT, the exogenous EBR-L group reached full bloom, with a flowering rate significantly higher than that of the CK group (Figure 5C,D). These results showed that exogenous EBR-L accelerated flowering, whereas exogenous EBR-H delayed flowering in both AF1 and SF3.

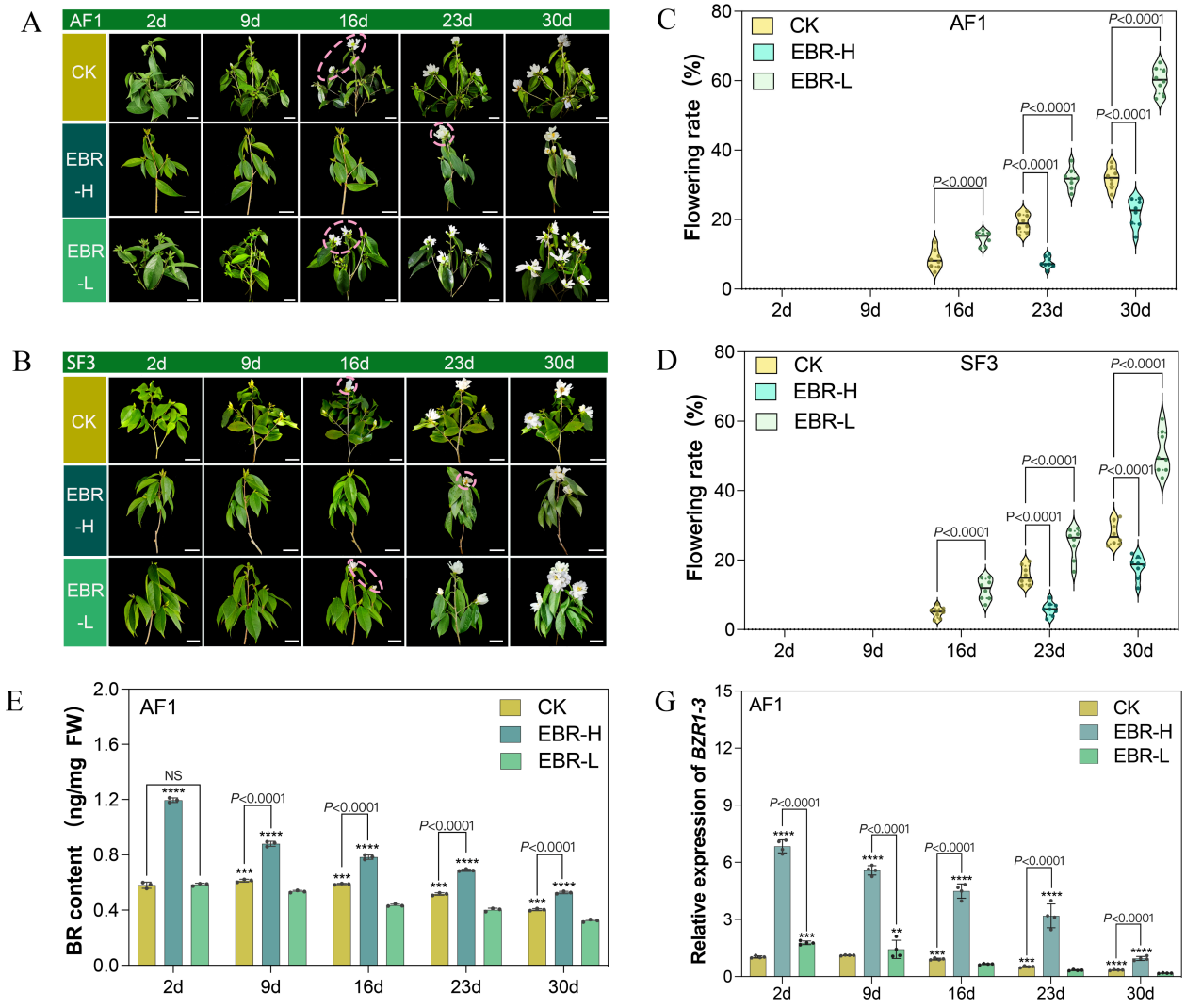


Figure 5. *Cont.*

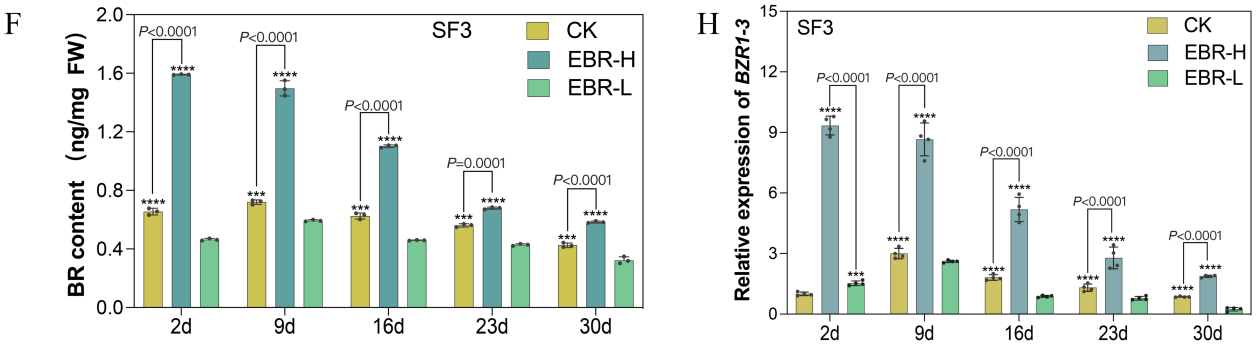


Figure 5. Effects of exogenous BR treatments on flowering rate, BR content, and *BZR1-3* expression in AF1 and SF3. (**A**,**B**) Flowering phenotypes of AF1 and SF3 under exogenous BR treatments at 2, 9, 16, 23, and 30 days after treatments (DAT). EBR-L: low-concentration (L, 0.5 mg/L), EBR-H: high-concentration (H, 2 mg /L). Scale bar, 8 cm. (**C**,**D**) Flowering rates of AF1 and SF3 under exogenous BR treatments at 2, 9, 16, 23, and 30 DAT. Data are presented as violin plots (shape, data distribution; inner line, median), and mean ± SD (n = 8). (**E**,**F**) BR content in AF1 and SF3 under exogenous BR treatments at 2, 9, 16, 23, and 30 DAT. Asterisks indicate significant differences (*** $p < 0.001$; **** $p < 0.0001$; one-way ANOVA with Tukey's HSD test; n = 3). (**G**,**H**) qRT-PCR analysis of *BZR1-3* expression in AF1 and SF3 floral buds under exogenous BR treatments. *EF1α* was used as the internal reference. Asterisks indicate significant differences (** $p < 0.01$; *** $p < 0.001$; **** $p < 0.0001$; one-way ANOVA with Tukey's HSD test; n = 4).

We further quantified the BR content following exogenous EBR treatments in both AF1 and SF3. As the ELISA method cannot distinguish between plant-derived BR and applied exogenous EBR, the following measurements are referred to as assay-defined BR immunoreactivity. Under the exogenous EBR-H treatments, BR surged initially and then gradually declined, but remained significantly higher than that in the CK and EBR-L groups across all five time points ($p < 0.0001$). In contrast, exogenous EBR-L treatments significantly reduced BR content compared with the CK during the subsequent stages (9 to 30 DAT) in AF1, whereas a sustained reduction was observed across all five time points in SF3. Notably, under exogenous EBR-H treatments, the BR levels in SF3 were significantly higher than those in AF1 (Figure 5E,F). These results suggested that exogenous EBR-L downregulated BR content, whereas exogenous EBR-H upregulated BR content in both AF1 and SF3.

We further quantified the *BZR1-3* expression abundance following exogenous EBR treatments in both AF1 and SF3. The expression of *BZR1-3* was strongly induced by EBR-H treatments in both AF1 and SF3, maintaining significantly higher expression levels than CK and EBR-L groups across all five time points ($p < 0.0001$). Notably, under EBR-H treatments, the *BZR1-3* expression level in SF3 was consistently higher than that in AF1. In contrast, under EBR-L treatments, the *BZR1-3* expression level was slightly higher than or comparable to the CK at the early stages (2 to 9 DAT), but became consistently lower than the CK at the later stages (16 to 30 DAT). This expression pattern was consistent with the observed changes in BR levels and was inversely correlated with the flowering rate (Figure 5G,H). Collectively, these results suggest an association between BR and *BZR1-3* expression, with elevated BR correlating with its upregulation and delayed flowering.

4. Discussion

Woody perennials enter seasonal dormancy to avoid unfavorable environmental conditions [34]. The dormancy classification system divides dormancy into three distinct phases: paradormancy (dominance-mediated suppression), endodormancy (internally regulated dormancy), and ecodormancy (externally imposed dormancy) [35]. Plant bud dormancy is an adaptive characteristic in response to harsh conditions [36], ensuring the preservation of

flower buds and facilitating robust growth, flowering, and fruit in the following year [37,38]. For example, in apple (*Malus* × *domestica* 'Royal Gala'), floral bud dormancy delayed budbreak and altered bud architecture due to constrained lateral shoot outgrowth, but normal flower and fruit development [39]. In poplar (*Populus alba* × *Populus glandulosa*), floral buds enter dormancy in winter, enhancing stress adaptability [40]. In this study, we identified that autumn–winter and spring flowering ecotypes experienced morphological synchrony in reproductive development. In the spring-flowering ecotype SF3, floral buds enter a dormant phase after completing differentiation and remain unopened throughout the winter. This progression aligns with the dormancy transition described in perennial woody plants [41]. This prolonged suspension of floral development is subsequently released with the onset of spring, triggering synchronized bloom. In contrast, the autumn–winter flowering ecotype AF1 bypasses this prolonged dormant phase, with floral buds transitioning directly to full bloom at P5.

The coordinated interplay among phytohormones and plant growth regulators ensures precise transcriptional regulation, normal plant growth and development, and environmental adaptation [39]. Hydrogen cyanamide (HC) has been shown to advance flowering in oil camellias (*Camellia oleifera Abel.*) by promoting cell expansion, cell cycle progression, and floral organ development within floral buds [25]. Brassinosteroid (BR) is steroid plant hormone, which can protect plants from a variety of abiotic stresses, including drought, salt, heat, and cold stress [42]. In this study, elevated BR promoted dormancy and suppressed flowering in SF3, while reduced BR accelerated flowering in both AF1 and SF3. This regulatory pattern was further corroborated by studies in tea plants (*Camellia sinensis*), where elevated BR levels repressed flowering [19].

Exogenous BR can delay flowering in *Arabidopsis thaliana* ecotype *Wassilewskija-2*, and attenuated BR upregulates *FLC* to promote dormancy in mulberry (*Morus alba*) [43,44]. Here, exogenous EBR treatments verified this flowering regulatory pattern: 0.5 mg/L exogenous EBR reduced BR levels and accelerated flowering, whereas 2 mg/L exogenous EBR increased BR levels and delayed flowering in both AF1 and SF3. A similar concentration-dependent pattern has been observed in grape (*Vitis vinifera* L.), where low-concentration BR inhibited BR biosynthesis [45]. Together, these findings suggest that BR acts as a potential negative regulator of flowering through a concentration-dependent mechanism to maintain floral bud dormancy and suppress flowering. Furthermore, how exogenous EBR application differentially modulates endogenous BR synthesis and metabolism to exert this concentration-dependent control over floral bud dormancy and flowering warrants further investigation. We acknowledge that the control (CK) group was sprayed with distilled water only, without the addition of the equivalent ethanol solvent used in the EBR treatments. This represents a limitation of our study, as we cannot completely exclude the potential minor effects of the trace ethanol (<0.1%, v/v). Future studies should incorporate a solvent-matched (vehicle) control to further validate these findings.

Mechanistically, brassinosteroid (BR) signaling is transduced through a well-defined molecular pathway [15]. At the plasma membrane, the leucine-rich repeat receptor-like kinase BRI1 and its co-receptor BAK1 jointly perceive BR ligands [31,32], initiating an intracellular phosphorylation cascade that ultimately regulates the activity of key transcription factors BZR1 and BES1 via inhibition of the GSK3-like kinase BIN2 [14,18,46]. Here, we found that *BZR1-3* expression was significantly upregulated under high BR levels during the dormancy period in SF3 (P5). In addition, *BIN2* expression exhibited an inverse correlation with *BZR1-3* in both AF1 and SF3 [47]. This pattern mirrors observations in seed dormancy, where BR actively participates in balancing dormancy maintenance and release [48], suggesting a potentially conserved BZR1-centered regulatory association across dormant plant tissues [49]. Future studies incorporating epigenomic analyses will further elucidate

how this regulatory mechanism interacts with the epigenetic landscape in the regulation of control floral bud dormancy. In summary, we propose a working hypothesis that BR is associated with floral bud dormancy and flowering via the transcription factor BZR1-3. While our current data provide valuable macroscopic insights, a deeper understanding of the spatial distribution of BR and the epigenetic landscape will require future spatial and epigenomic approaches.

5. Conclusions

Our study provides evidence suggesting that brassinosteroid (BR) signaling is associated with floral bud dormancy and delayed flowering in oil camellias. Transcriptomic profiling and qRT-PCR analysis further identified BZR1-3 as a candidate transcription factor of the BR signaling pathway involved in dormancy-flowering transition. Exogenous high-concentration EBR (EBR-H) treatments elevated BR levels, leading to sustained transcript accumulation of *BZR1-3*, which was correlated with reinforced floral bud dormancy. Conversely, exogenous low-concentration EBR (EBR-L) treatments reduced BR accumulation and were associated with the progressive downregulation of *BZR1-3* at later stages, which is associated with flowering (Figure 6). Collectively, these findings suggest that BZR1-3 acts as a candidate transcription factor connecting BR to floral bud dormancy. This provides a foundation for future genetic studies to elucidate the flowering regulatory mechanism in oil camellias.

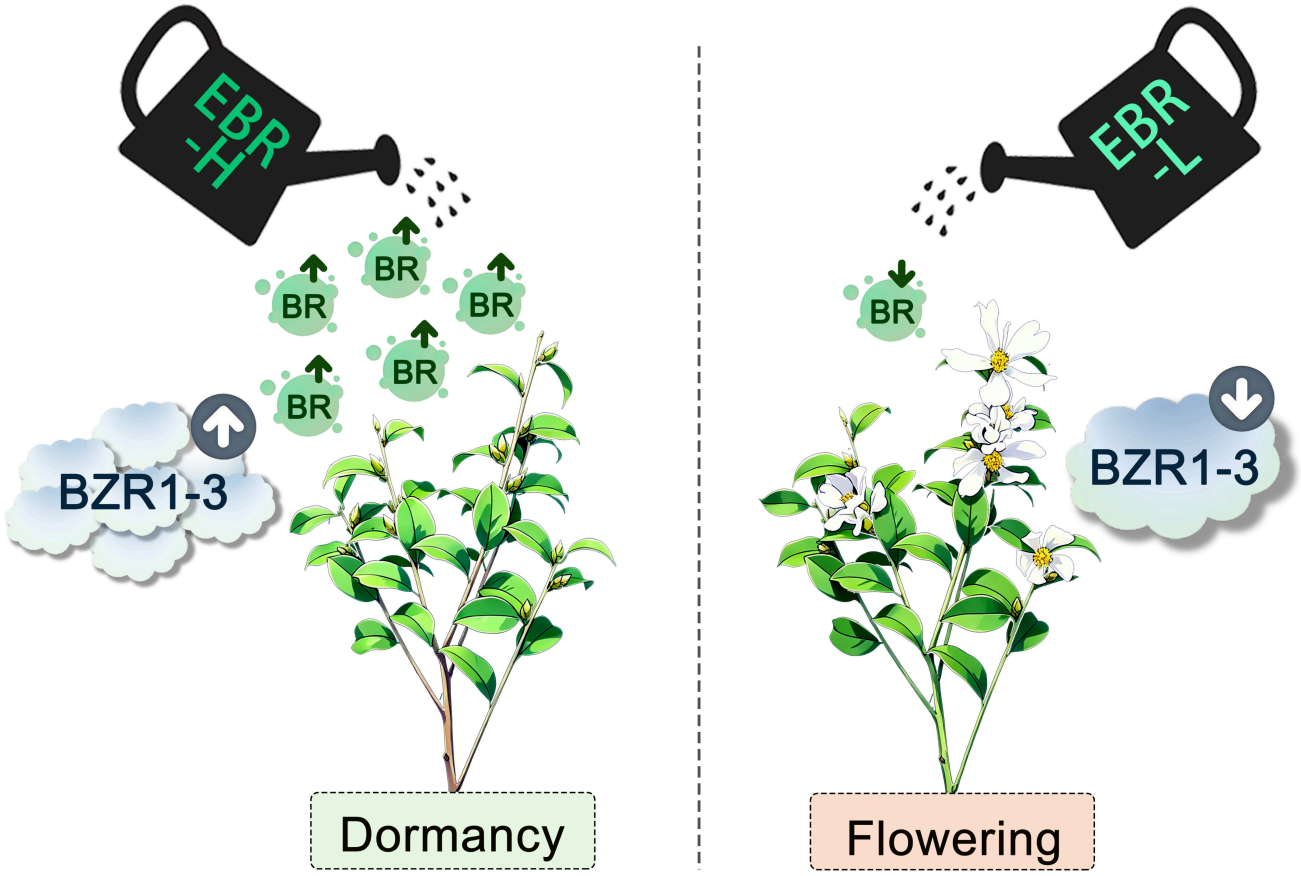


Figure 6. A hypothesized model illustrating how BR promotes floral bud dormancy and delays flowering. High-concentration EBR treatment (EBR-H) increases BR levels and upregulates *BZR1-3*, maintaining floral bud dormancy. In contrast, low-concentration EBR treatment (EBR-L) decreases BR levels and downregulates *BZR1-3*, facilitating the transition to flowering.

Supplementary Materials: The following supporting information can be downloaded at https://www.mdpi.com/article/10.3390/horticulturae12111438/s1, Figure S1. Principal component analysis (PCA) of transcriptome profiles across six developmental stages (P1–P6) in AF1 and SF3 floral buds.; Figure S2. Diagram of KEGG enrichment genes between AF1 and SF3 floral buds at P1.; Figure S3. Diagram of KEGG enrichment genes between AF1 and SF3 floral buds at P2; Figure S4. Diagram of KEGG enrichment genes between AF1 and SF3 floral buds at P3; Figure S5. Diagram of KEGG enrichment genes between AF1 and SF3 floral buds at P4; Figure S6. Diagram of KEGG enrichment genes between AF1 and SF3 floral buds at P5; Figure S7. Diagram of KEGG enrichment genes between P5 and P6 in SF3 floral buds; Figure S8. Comparison of key amino acid residues and motifs in BZR family proteins based on sequence alignment. The sequences shown include CsBZR1 from *Camellia sinensis*, At BZR1 from *Arabidopsis thaliana*, NtBZR1 from *Nicotiana tabacum*.

Author Contributions: Conceptualization, D.Y. and W.G.; methodology, H.Q.; software, J.F.; validation, H.Q. and Y.C.; formal analysis, H.Q.; investigation, H.Q., J.F. and Y.D.; resources, D.Y.; data curation, H.Q. and Y.D.; writing—original draft preparation, H.Q.; writing—review and editing, Y.C.; visualization, H.Q.; supervision, W.G.; project administration, W.G.; funding acquisition, D.Y. All authors have read and agreed to the published version of the manuscript.

Funding: This work was supported by the National Natural Science Foundation of China (32572101). Yuelushan Laboratory Breeding Program (YLS-2025-ZY02050).

Data Availability Statement: The original contributions presented in this study are included in the article/Supplementary Material. Further inquiries can be directed to the corresponding author.

Conflicts of Interest: These authors contributed equally to this work.

References

1. Yan, J.; Liu, Q.; Guo, P.; Wang, Y.; Sheng, S.; Liu, X.; Zhang, R.; Li, J.; Tan, X. Time-course transcriptome analysis unveils the CoFKF1-CoMYB4-CoFT1 regulatory module in flowering control of *camellia oleifera* abel. *Plant Cell Environ*. **2025**, *48*, 6153–6169. [CrossRef] [PubMed]
2. Andrés, F.; Coupland, G. The genetic basis of flowering responses to seasonal cues. *Nat. Rev. Genet*. **2012**, *13*, 627–639. [CrossRef] [PubMed]
3. Fournier-Level, A.; Taylor, M.A.; Paril, J.F.; Martínez-Berdeja, A.; Stitzer, M.C.; Cooper, M.D.; Roe, J.L.; Wilczek, A.M.; Schmitt, J. Adaptive significance of flowering time variation across natural seasonal environments in *Arabidopsis thaliana*. *New Phytol*. **2022**, *234*, 719–734. [CrossRef] [PubMed]
4. Wu, T.; Liu, Z.; Yu, T.; Zhou, R.; Yang, Q.; Cao, R.; Nie, F.; Ma, X.; Bai, Y.; Song, X. Flowering genes identification, network analysis, and database construction for 837 plants. *Hortic. Res*. **2024**, *11*, uhae013. [CrossRef] [PubMed]
5. Pandey, S.K.; Moraes, T.S.; Nair, A.; Aryal, B.; Azeez, A.; Miskolczi, P.; Maucort, G.; Cordelières, F.P.; Brocard, L.; Davis, G.V.; et al. Variable temperature processing by plasmodesmata regulates robust bud dormancy release. *Nat. Commun*. **2026**, *17*, 348. [CrossRef] [PubMed]
6. Gao, Y.; Yang, Q.; Yan, X.; Wu, X.; Yang, F.; Li, J.; Wei, J.; Ni, J.; Ahmad, M.; Bai, S.; et al. High-quality genome assembly of "Cuiguan" pear (*Pyrus pyrifolia*) as a reference genome for identifying regulatory genes and epigenetic modifications responsible for bud dormancy. *Hortic. Res*. **2021**, *8*, 197. [CrossRef] [PubMed]
7. Horvath, D.P.; Anderson, J.V.; Chao, W.S.; Foley, M.E. Knowing when to grow: Signals regulating bud dormancy. *Trends Plant Sci.* **2003**, *8*, 534–540. Correction in *Trends Plant Sci*. **2003**, *9*, 12. https://doi.org/10.1016/j.tplants.2003.11.005. [CrossRef] [PubMed]
8. Janice, E.K. COOKE The dynamic nature of bud dormancy in trees: Environmental control and molecular mechanisms. *Plant Cell Environ*. **2012**, *35*, 1707–1728. [CrossRef] [PubMed]
9. Azeez, A.; Zhao, Y.C.; Singh, R.K.; Yordanov, Y.S.; Dash, M.; MiskolSczi, P.; Stojkovič, K.; Strauss, S.H.; Bhalerao, R.P.; Busov, V.B. EARLY BUD-BREAK 1 and EARLY BUD-BREAK 3 control resumption of poplar growth after winter dormancy. *Nat. Commun*. **2021**, *12*, 1123. [CrossRef] [PubMed]
10. Kazan, K.; Lyons, R. The link between flowering time and stress tolerance. *J. Exp. Bot*. **2016**, *67*, 47–60. [CrossRef] [PubMed]
11. Rinne, P.L.H.; Welling, A.; Vahala, J.; Ripel, L.; Ruonala, R.; Kangasjärvi, J.; Van Der Schoot, C. Chilling of dormant buds hyperinduces *FLOWERING LOCUS T* and recruits GA-inducible 1,3-β-glucanases to reopen signal conduits and release dormancy in *populus*. *Plant Cell* **2011**, *23*, 130–146. [CrossRef] [PubMed]
12. Zhao, Y.; Li, Y.; Guo, D.; Chen, X.; Cao, K.; Wu, J.; Fang, W.; Chen, C.; Wang, X.; Wang, L. Spatiotemporally transcriptomic analyses of floral buds reveal the high-resolution landscape of flower development and dormancy regulation in peach. *Hortic. Res*. **2025**, *12*, uhaf029. [CrossRef] [PubMed]

13. Wei, J.; Yang, Q.; Ni, J.; Gao, Y.; Tang, Y.; Bai, S.; Teng, Y. Early defoliation induces auxin redistribution, promoting paradormancy release in pear buds. *Plant Physiol.* **2022**, *190*, 2739–2756. Correction in *Plant Physiol.* **2023**, *191*, 2066. [CrossRef] [PubMed]
14. He, J.-X.; Gendron, J.M.; Sun, Y.; Gampala, S.S.L.; Gendron, N.; Sun, C.Q.; Wang, Z.-Y. BZR1 is a transcriptional repressor with dual roles in brassinosteroid homeostasis and growth responses. *Science* **2005**, *307*, 1634–1638. [CrossRef] [PubMed]
15. Clouse, S.D. The molecular intersection of brassinosteroid-regulated growth and flowering in *Arabidopsis*. *Proc. Natl. Acad. Sci. USA* **2008**, *105*, 7345–7346. [CrossRef] [PubMed]
16. Hong, J.; Lee, H.; Lee, J.; Kim, H.; Ryu, H. ABSCISIC ACID-INSENSITIVE 3 is involved in brassinosteroid-mediated regulation of flowering in plants. *Plant Physiol. Biochem.* **2019**, *139*, 207–214. [CrossRef] [PubMed]
17. Dai, X.; Zhang, Y.; Xu, X.; Ran, M.; Zhang, J.; Deng, K.; Ji, G.; Xiao, L.; Zhou, X. Transcriptome and functional analysis revealed the intervention of brassinosteroid in regulation of cold induced early flowering in tobacco. *Front. Plant Sci.* **2023**, *14*, 1136884. [CrossRef] [PubMed]
18. Liu, Y.; Zhang, H.; Feng, W.; Lin, X.; Gao, A.; Cao, Y.; Yang, Q.; Wang, Y.; Li, W.; Fu, F.; et al. The maize ZmBES1/BZR1-9 transcription factor accelerates flowering in transgenic arabidopsis and rice. *Plants* **2023**, *12*, 2995. [CrossRef] [PubMed]
19. Zhang, Y.; Li, H.; Wan, S.; Zhang, Y.; Chen, D.; Zhang, H.; Xiao, Y.; Liu, L.; Wang, P.; Yu, Y. Brassinosteroid signaling regulates floral transition defects in *camellia sinensis* 'ziyang 1' via CsBZR2-mediated suppression of CsFLC. *J. Integr. Agric.* **2025**, *25*, 4208–4222. [CrossRef]
20. Song, Q.; Gong, W.; Yu, X.; Ji, K.; Jiang, Y.; Chang, Y.; Yuan, D. Transcriptome and anatomical comparisons reveal the effects of methyl jasmonate on the seed development of *camellia oleifera*. *J. Agric. Food Chem.* **2023**, *71*, 6747–6762. [CrossRef] [PubMed]
21. Zhang, D.; Stack, L.; Chen, Y.; Zhang, R.; Yu, J.; Xie, B.; Ruter, J.M. Tea oil Camellia—Eastern "Olive" for the World. *Acta Hortic.* **2008**, *769*, 43–48.
22. Ebadi, A.; Coombe, B.G.; May, P. Fruit-set on small chardonnay and shiraz vines grown under varying temperature regimes between budburst and flowering. *Aust. J. Grape Wine Res.* **1995**, *1*, 3–10. [CrossRef]
23. Wang, Y.-J.; Wu, L.-L.; Sun, M.; Li, Z.; Tan, X.-F.; Li, J.-A. Transcriptomic and metabolomic insights on the molecular mechanisms of flower buds in responses to cold stress in two *Camellia oleifera* cultivars. *Front. Plant Sci.* **2023**, *14*, 1126660. [CrossRef] [PubMed]
24. Song, H.; Duan, Z.; Huo, H.; Wang, X.; Wang, Y.; Chen, J.; Jin, L.; Lin, M. A global overview of transcriptome dynamics during the late stage of flower bud development in *Camellia oleifera*. *BMC Plant Biol.* **2025**, *25*, 247. [CrossRef] [PubMed]
25. Lin, M.; Wang, S.; Liu, Y. Hydrogen cyanamide enhances flowering time in tea oil camellia (*Camellia oleifera* Abel.). *Ind. Crops Prod.* **2022**, *176*, 114313. [CrossRef]
26. Goodwin, E.K.; Rader, R.; Encinas-Viso, F.; Saunders, M.E. Weather conditions affect the visitation frequency, richness and detectability of insect flower visitors in the australian alpine zone. *Environ. Entomol.* **2021**, *50*, 348–358. [CrossRef] [PubMed]
27. Chang, Y.; Gong, W.; Xu, J.; Gong, H.; Song, Q.; Xiao, S.; Yuan, D. Integration of semi- *in vivo* assays and multi-omics data reveals the effect of galloylated catechins on self-pollen tube inhibition in *Camellia oleifera*. *Hortic. Res.* **2023**, *10*, uhac248. [CrossRef] [PubMed]
28. Wu, L.-L.; Wang, Y.; Guo, P.; Li, Z.; Li, J.-A.; Tan, X.-F. Metabonomic and transcriptomic analyses of *Camellia oleifera* flower buds treated with low-temperature stress during the flowering stage. *Ind. Crops Prod.* **2022**, *189*, 115874. [CrossRef]
29. Zhang, L.; Shi, Y.; Gong, W.; Zhao, G.; Xiao, S.; Lin, H.; Li, Y.; Liao, Z.; Zhong, S.; Hu, G.; et al. The tetraploid *Camellia oleifera* genome provides insights into evolution, agronomic traits, and genetic architecture of oil Camellia plants. *Cell Rep.* **2024**, *43*, 114902. [CrossRef] [PubMed]
30. Ding, J.; Wang, K.; Pandey, S.; Perales, M.; Allona, I.; Khan, M.R.I.; Busov, V.B.; Bhalerao, R.P. Molecular advances in bud dormancy in trees. *J. Exp. Bot.* **2024**, *75*, 6063–6075. [CrossRef] [PubMed]
31. Oh, M.-H.; Wang, X.; Kota, U.; Goshe, M.B.; Clouse, S.D.; Huber, S.C. Tyrosine phosphorylation of the BRI1 receptor kinase emerges as a component of brassinosteroid signaling in *Arabidopsis*. *Proc. Natl. Acad. Sci. USA* **2009**, *106*, 658–663. [CrossRef] [PubMed]
32. Li, J.; Wen, J.; Lease, K.A.; Doke, J.T.; Tax, F.E.; Walker, J.C. BAK1, an Arabidopsis LRR Receptor-like Protein Kinase, Interacts with BRI1 and Modulates Brassinosteroid Signaling. *Cell* **2002**, *110*, 213–222. [CrossRef] [PubMed]
33. Yin, Y.; Wang, Z.-Y.; Mora-Garcia, S.; Li, J.; Yoshida, S.; Asami, T.; Chory, J. BES1 accumulates in the nucleus in response to brassinosteroids to regulate gene expression and promote stem elongation. *Cell* **2002**, *109*, 181–191. [CrossRef] [PubMed]
34. Liu, J.; Sherif, S.M. Hormonal orchestration of bud dormancy cycle in deciduous woody perennials. *Front. Plant Sci.* **2019**, *10*, 1136. [CrossRef] [PubMed]
35. Lang, G.A.; Early, J.D.; Martin, G.C.; Darnell, R.L. Endo-, Para-, and Ecodormancy: Physiological Terminology and Classification for Dormancy Research. *HortScience* **1987**, *22*, 371–377. [CrossRef]
36. Zhao, Y.; Ma, Y.; Qiu, H.; Zhou, L.; He, K.; Ye, Y. Wake up: The regulation of dormancy release and bud break in perennial plants. *Front. Plant Sci.* **2025**, *16*, 1553953. [CrossRef] [PubMed]
37. Penfield, S. Beyond floral initiation: The role of flower bud dormancy in flowering time control of annual plants. *J. Exp. Bot.* **2024**, *75*, 6056–6062. [CrossRef] [PubMed]

38. Lu, X.; O'Neill, C.M.; Warner, S.; Xiong, Q.; Chen, X.; Wells, R.; Penfield, S. Winter warming post floral initiation delays flowering via bud dormancy activation and affects yield in a winter annual crop. *Proc. Natl. Acad. Sci. USA* **2022**, *119*, e2204355119. [CrossRef] [PubMed]
39. Wu, R.; Tomes, S.; Karunairetnam, S.; Tustin, S.D.; Hellens, R.P.; Allan, A.C.; Macknight, R.C.; Varkonyi-Gasic, E. SVP-like MADS Box Genes Control Dormancy and Budbreak in Apple. *Front. Plant Sci.* **2017**, *08*, 477. [CrossRef] [PubMed]
40. Yoon, S.-K.; Bae, E.-K.; Choi, H.; Choi, Y.-I.; Lee, H. Isolation and Expression of Dormancy-associated protein 1 (DRM1) in Poplar (*Populus alba* × *P. glandulosa*). *Plant Biotechnol. J.* **2017**, *44*, 69–75. Correction in *Plant Biotechnol. J.* **2017**, *44*, 207. https://doi.org/10.5010/JPB.2017.44.3.207. [CrossRef]
41. Rohde, A.; Bhalerao, R.P. Plant dormancy in the perennial context. *Trends Plant Sci.* **2007**, *12*, 217–223. [CrossRef] [PubMed]
42. Barrero-Gil, J.; Salinas, J. CBFs at the Crossroads of Plant Hormone Signaling in Cold Stress Response. *Mol. Plant* **2017**, *10*, 542–544. [CrossRef] [PubMed]
43. Domagalska, M.A.; Schomburg, F.M.; Amasino, R.M.; Vierstra, R.D.; Nagy, F.; Davis, S.J. Attenuation of brassinosteroid signaling enhances *FLC* expression and delays flowering. *Development* **2007**, *134*, 2841–2850. [CrossRef] [PubMed]
44. Janeczko, A.; Filek, W.; Biesaga-Koscielniak, J.; Marcinska, I.; Janeczko, Z. The influence of animal sex hormones on the induction of flowering in *Arabidopsis thaliana*: Comparison with the effect of 24-epibrassinolide. *Plant Cell Tissue Organ Cult. PCTOC* **2003**, *72*, 147–151. [CrossRef]
45. Xu, F.; Xi, Z.; Zhang, H.; Zhang, C.; Zhang, Z. Brassinosteroids are involved in controlling sugar unloading in Vitis vinifera 'Cabernet Sauvignon' berries during véraison. *Plant Physiol. Biochem.* **2015**, *94*, 197–208. [CrossRef] [PubMed]
46. Bai, Q.; Wang, L.; Huang, S.; Ali, K.; Li, G.; Ren, H.; Zheng, B. The receptor-like kinase EMS1 and BRI1 coordinately regulate stamen elongation via the transcription factors BES1/BZR1 in Arabidopsis. *Plant Sci.* **2023**, *331*, 111673. [CrossRef] [PubMed]
47. Yan, Z.; Zhao, J.; Peng, P.; Chihara, R.K.; Li, J. BIN2 functions redundantly with other arabidopsis GSK3-like kinases to regulate brassinosteroid signaling. *Plant Physiol.* **2009**, *150*, 710–721. [CrossRef] [PubMed]
48. Kumar, V.; Jaiswal, D.K.; Ansari, W.A.; Sahu, P.K.; Kumar Baranwal, V. Unveiling nature's dormancy code: The pivotal role of brassinosteroids in seed germination. *J. Plant Growth Regul.* **2026**, *45*, 3561–3574. [CrossRef]
49. Zuo, C.; Zhang, L.; Yan, X.; Guo, X.; Zhang, Q.; Li, S.; Li, Y.; Xu, W.; Song, X.; Wang, J.; et al. Evolutionary analysis and functional characterization of BZR1 gene family in celery revealed their conserved roles in brassinosteroid signaling. *BMC Genom.* **2022**, *23*, 568. [CrossRef] [PubMed]

Disclaimer/Publisher's Note: The statements, opinions and data contained in all publications are solely those of the individual author(s) and contributor(s) and not of MDPI and/or the editor(s). MDPI and/or the editor(s) disclaim responsibility for any injury to people or property resulting from any ideas, methods, instructions or products referred to in the content.